5 Advanced Virgo: interferometer configuration

5.1 Introduction

This section describes the optical parameters and configuration of the AdV interferometer. The optical layout and the main parameters of the design are briefly summarised first, followed by a more detailed description of selected topics.

The design of the AdV core interferometer falls within the scope of the *Optical Simulation and Design* (OSD) subsystem. The optical layout and the nomenclature of the core interferometer, including the Michelson interferometer, its arm cavities and the mirrors forming the Power- and Signal-Recycling cavities is shown in Figure 13. Compared to the optical layout of Virgo, the AdV design features three main changes: the inclusion of Signal Recycling, the change in the arm cavities' geometry from a flat-concave to near-symmetric design and the move from marginally stable recycling cavities to non-degenerate recycling cavities. These topics will be described in more details in the following sections.

5.1.1 Optical layout

The optical layout of the main interferometer in the current AdV baseline design is shown in Figure 13, with the main or core interferometer being defined as the long-baseline Michelson interferometer formed by the central beam splitter (BS) with arm cavities (X-arm and Y-arm) and the so-called recycling mirrors (PRM, SRM) in the input and output ports of the Michelson interferometer. This optical layout is essentially the same as the Advanced LIGO design.

The laser light, after being filtered by the input mode-cleaner (IMC, not shown in this figure), is injected into the interferometer through the semi-transparent Power-Recycling mirror. Arm cavities as well as the Power-recycling mirror are used to enhance the light power circulating in the arm because the signal-to-shotnoise ratio of the optical readout scales with the square root of the circulating power. The main output port of the interferometer is the so-called *asymmetric port* (AP), with the Michelson set such that this port is on the dark fringe. Before being detected on a high-power photo diode the signal is optically enhanced and filtered in the Signal Recycling cavity (formed by SRM1 and the Michelson) and then spatially filtered by a small rigid mode-cleaner cavity (OMC). The other optical outputs depicted by photo-diodes in figure 13 are detection ports that can potentially be used for interferometer control or monitoring purposes.

5.1.2 Design summary

The current configuration of the main interferometer is defined by the parameters given in table 7. This section provides a brief explanation of the optical parameters, in the same order as following sections with a more detailed description.
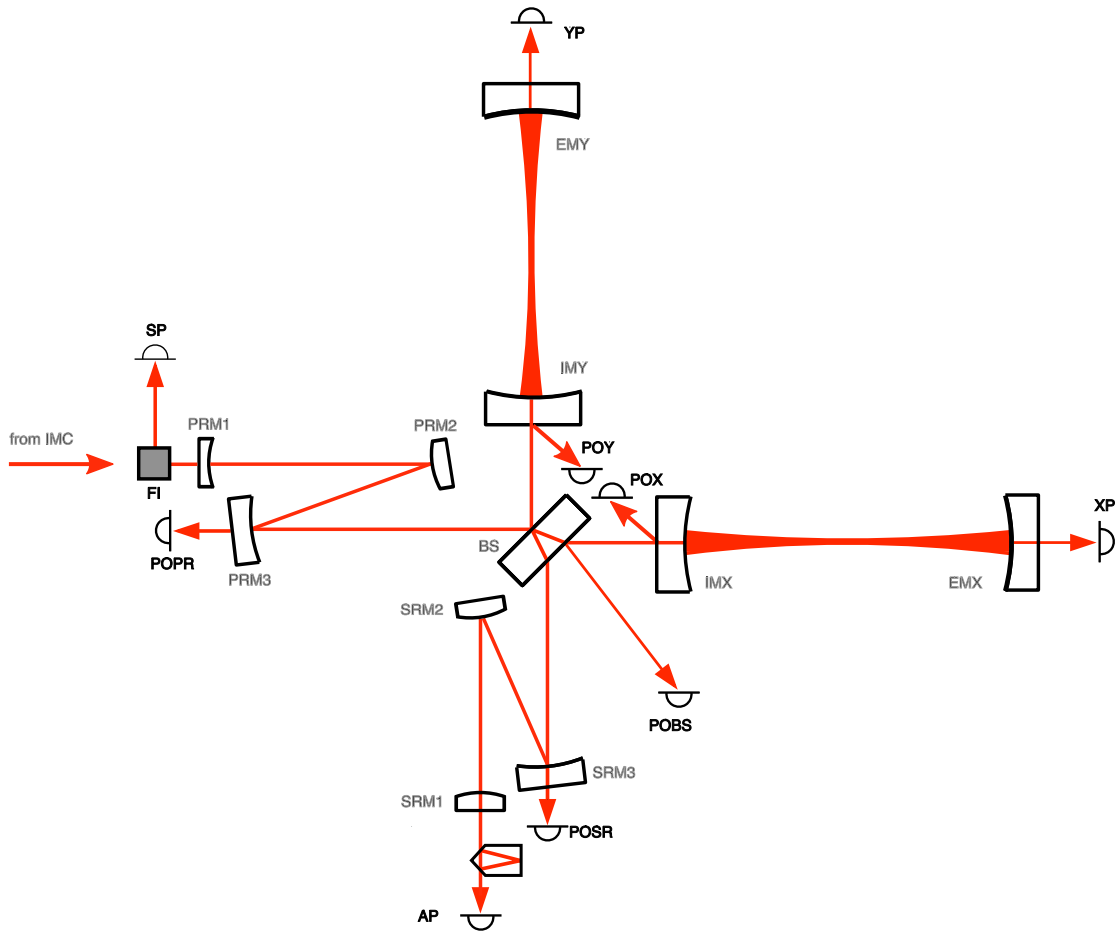
Figure 13: Optical layout of the AdV core interferometer: A new, clear nomenclature has been chosen [118] for Advanced VIRGO in order to avoid inconsistencies and possible confusion with the ongoing work on the Virgo interferometer: The interferometer arms will be identified by the letters *X* and *Y*, with the North arm, in-line with the input beam, being the X-arm. Cavity mirrors are called input mirror (IM) or end mirror (EM). Thus the North arm cavity (X arm) is formed by IMX and EMX. The recycling mirrors are called power recycling mirror (PRM) and signal recycling mirror (SRM). The dark fringe output port the Michelson interferometer is the *asymmetric port* (AP). The *symmetric port* (SP) denotes the back reflection from the Michelson (in-line with the X-Arm). Other readout ports are named after the optical component providing the beam: the light transmitted by the X-Arm cavity is called XP. So-called 'pick-off' beams will be labelled with *PO*, i.e. the reflection from the anti-reflective coating of the beam splitter will be detected in POBS. The folded optical path inside the Power- and Signal Recycling cavities increase the cavity lengths, which is required to achieve non-degeneracy for these cavities. The curvatures of the Recycling mirrors and of the folding mirrors are determined by cavity length and the required Gouy phase, see section 5.5.

Light power   The light power circulating in the arms is maximised by increasing either the finesse of the arm cavity and/or the finesse of the Power Recycling cavity (see below) to reduce shotnoise.

Arm cavity geometry   Both arm cavities have the same geometry, with the beam waist being close to the center of the cavity. This minimizes the thermal noise contribution. Care has been taken to reach a stable cavity suppressing higher-order modes.

Arm cavity finesse   Both cavities have the same finesse. High-finesse cavities help to reduce shotnoise and have advantages with respect to noise suppression but are limited by losses in the cavity which are difficult to predict accurately. Currently we have based the finesse on the assumption of very low losses, this might be adjusted later, depending on results from an ongoing R+D program.

Geometry of mirror and beam splitter substrates   The size of the mirrors should be as large as possible to minimise thermal noise and is limited by technical constraints. The thickness does not influence the optical design. So far, no decision has been taken regarding wedges in the substrate. In some configurations wedges can create extra pick-off beams or can help to separate such beams from the main beam.

Power Recycling cavity   The Power Recycling mirror is used to further enhance the circulating light power and thus to reduce shotnoise. The finesse of the cavity is designed following the arm cavity finesse. The current design features a non-degenerate cavity with two turning mirrors and a folded path. This design should make the interferometer more robust against thermal deformations and misalignments.

Signal Recycling cavity   The Signal Recycling mirrors allows to tune and shape the quantum noise limited sensitivity of the detector; the SRC finesse affects the detector bandwidth and the SRM tuning the frequency of the peak sensitivity. The only drawback of Signal Recycling is a more complex control system. Also the Signal Recycling cavity is designed to be non-degenerate.

AdV Optical Configuration			
Light Power			
arm cavity power	760 kW	power on BS	2.7 kW
Arm cavity geometry			
cavity length L	3000 m		
IM R_C	1416 m	EM R_C	1646 m
Beam size IM w	56 mm	Beam size EM w	65 mm
waist size w_0	8.5 mm	waist position z	1385 m
Arm cavity finesse			
finesse	900	round-trip losses	75 ppm
transmission IM T	0.7%	transmission EM T	5 ppm
Power recycling			
transmission PRM T	4.6%	finesse	70
PRC length	24 m	Beam size on PRM1	1.8 mm
Signal recycling			
transmission SRM T	11%	finesse	40
SRC length	TBD	SRM tuning	0.15 rad
Mirrors			
IM diameter	35 cm	EM diameter	35 cm
IM thickness	20 cm	EM thickness	20 cm
IM wedge	TBD	EM wedge	TBD

Table 7: Parameters of the AdV interferometer. Some parameters cannot be given yet (TBD) but will be determined at a later stage, see text. Throughout the text we quote numerical values for several optical parameters. In many cases the exact value for such parameters will be adjusted during later stages of the design or during implementation. Therefore the values given in this table have been rounded to a few significant digits.

5.2 Beam size and waist position in the arm cavities

The size and shape of the laser beam inside the interferometer is defined by the surface shape of the cavity mirrors; the beam sizes at the IM and EM as well as the position of the cavity waist are determined by only two parameters, the radii of curvature (ROC) of IM and EM. Since inside the two Fabry-Perot cavities of the Michelson interferometer the GW interacts with the laser light, creating signal sidebands, the two arm cavities can be seen as the heart of the AdV detector. The characteristics of the arm cavities have not only a high impact on the detector sensitivity and bandwidth, but also on the overall detector performance. Therefore a thorough design of the ROCs, taking all relevant aspects into account, is of high importance.

In order to find the optimal ROC values a trade off analysis needs to be performed taking into account the following aspects:

- Coating Brownian noise

- Clipping losses of the mirrors

- Mode-Non-Degeneracy

5.2.1 Coating Brownian noise

The power spectral density, $S_x(f)$, of the coating Brownian noise can be expressed as [126]:

$$S_x(f) = \frac{4k_{\mathrm{B}}T}{\pi^2 fY} \frac{d}{r_0^2} \left(\frac{Y'}{Y}\phi_\parallel + \frac{Y}{Y'}\phi_\perp \right) \tag{15}$$

where f is the frequency, d the total thickness of the coating, r_0 describes the beam radius, Y and Y' are the Young's Modulus values for the substrate and coating respectively. $\phi_\parallel$ and $\phi_\perp$ are the mechanical loss values for the coating for strains parallel and perpendicular to the coating surface.

As indicated by Equation 15 the amplitude spectral density of the coating Brownian noise decreases proportional to the beam radius, r_0, at the mirror. Since the contribution from the coating Brownian noise (together with the quantum noise) directly limits the AdV sensitivity in the mid-frequency range (see Figure 2), the overall detector sensitivity increases with larger beam size at the IM and EM. That is the reason for moving the cavity waist from the IM (where it is placed in initial Virgo) towards the center of the arm cavity, resulting in roughly equal beam sizes at the IM and EM.

In addition one can see from Equation 15 that the amplitude spectral density of the coating Brownian noise of a mirror is proportional to the square root of the coating thickness. Due to the fact that for the very high reflectance of the EM a thicker coating is required than for the IM, the coating noise contribution of the EM would be higher than the one of the IM (assuming identical beam sizes). However, the lowest overall coating thermal noise of all four IM and EM is obtained for equal coating noise contribution of

all four mirrors. This can be achieved by positioning the cavity waist not directly in the center of the arm cavities, but slightly shifted towards the IM.

5.2.2 Clipping losses of the mirrors

As shown above the AdV sensitivity can be improved by increasing the beam size at the main test masses of the Fabry-Perot cavities. However, technical constraints, such as the actual size of the dielectric coatings or the free apertures of the reference masses limit the maximum beam size for a certain amount of tolerable clipping losses.

There are two problems connected to clipping losses: If the laser beam is too large for the mirror or its coating some light will be clipped, thus reducing the achievable power enhancement inside the interferometer. In addition if the clipped light is not properly destroyed or dumped, it might cause scattred light noise.

A detailed analysis of the maximal coating size to beam size ratio can be found in [127]. For the baseline mirror diameter of 35 cm clipping losses are going to limit the maximum beam radius at the test masses to about 5.0 to 6.5 cm.

5.2.3 Mode-Non-Degeneracy

In order to prevent light to be scattered into higher order optical modes (HOM) it is important to choose the mirror ROCs in a way to ensure that no lower order HOM is resonant inside the arm cavities. Furthermore, considering inevitable manufacturing inaccuracies of the ROC, we have to find ROC values sufficiently separated from the resonances.

In the following we will define a figure of merit for the cavity non-degeneracy. The Gouy phase of the HOM of the order k is defined as [128]:

$$\phi_k = k\frac{1}{\pi}\arccos\sqrt{(1 - \frac{L}{R_{c,i}})(1 - \frac{L}{R_{c,e}})}. \tag{16}$$

with L being the length of the arm cavity and $R_{c,i}$ and $R_{c,e}$ being the radii of curvature of the input and the end mirrors, respectively. The mode-non-degeneracy for a single HOM of the order k, Ψ_k, can then be expressed as follows:

$$\Psi_k(L, R_{c,i}, R_{c,e}) = |\phi_k - \text{round}(\phi_k)|. \tag{17}$$

In case Ψ_k equals zero any optical mode of the order k is degenerate with respect to the fundamental (TEM$_{00}$) mode. Finally in order tor provide a comprehensive figure of merit for the non-degeneracy of a cavity we have to combine the Ψ_k for all different HOM of interest. Taking into account all HOM up to the order N, we can now calculate the inverse quadratic sum of the individual $1/\Psi_k^2$ weighted by a factor $1/k!$:

$$\Theta_N(L, R_{c,i}, R_{c,e}) = \frac{1}{\sqrt{\sum_{k=1}^{N} \frac{1}{\Psi_k^2}\frac{1}{k!}}} \tag{18}$$
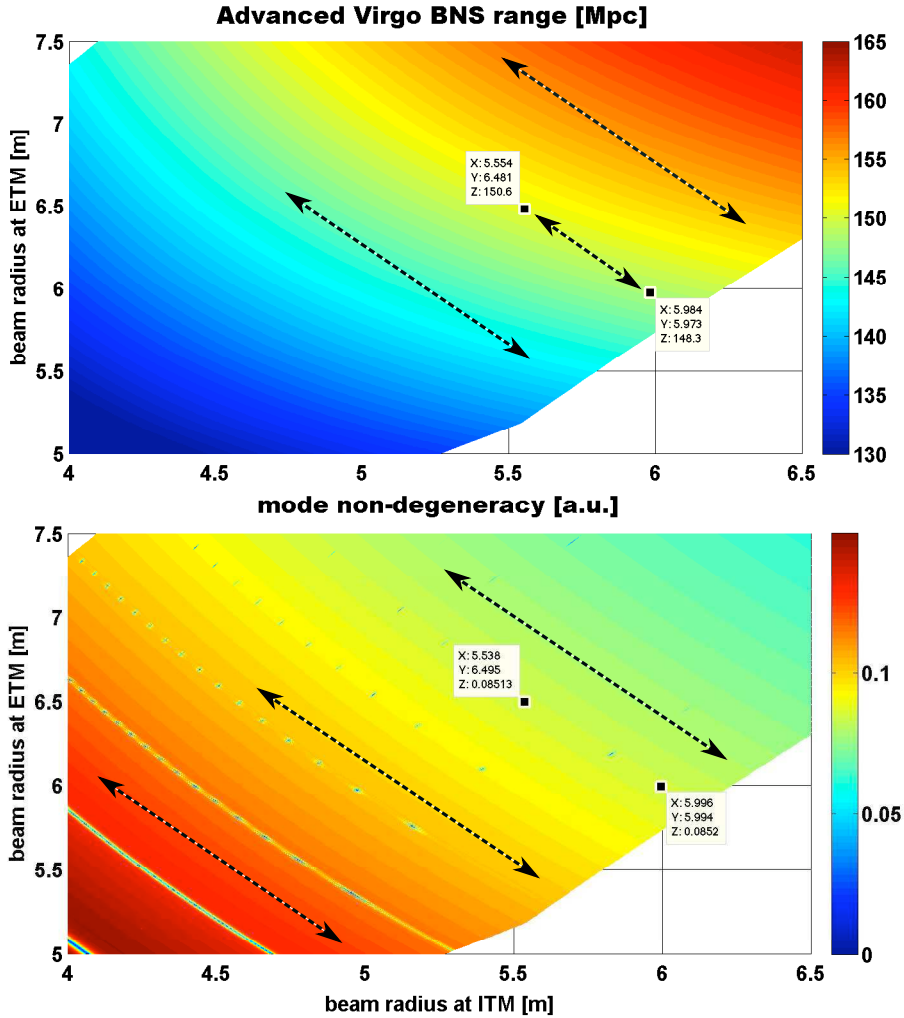
Figure 14: The lower subplot shows the mode-non-degeneracy in the arm cavities. Areas of the same color represent beam sizes combinations with identical cavity stability. As indicated by the dashed arrows one can move along a color boundary and keep the cavity stability at the same level. The upper subplot shows the achievable sensitivity, i.e. the BNS-range for AdV depending on the beam sizes. Again areas of same color indicate identical sensitivity. The orientation of the terraces for the non-degeneracy and the sensitivity is found to be different. This is why it is possible to improve the sensitivity, while keeping the cavity stability constant by following the black arrows in the upper subplot towards the upper left corner.

	input mirror	end mirror
beam radius [mm]	56	65
ROC [m]	1416	1646

Table 8: Design parameter of the AdV arm cavity geometry.

Θ_N can then be used as figure of merit for the non-degeneracy of the Advanced Virgo arm cavity design.

5.2.4 Trade-off of sensitivity and mode-non-degeneracy

Figure 14 shows an illustrative example of the trade off analysis required to choose the optimal beam sizes for advanced Virgo. In the upper subplot a scan of the figure of merit for the detector sensitivity, i.e. the binary neutron star inspiral (BNS) range versus the beam size at input and end mirrors is displayed. (This analysis uses the noise models described in [6] and the Signal-Recycling configuration optimized for maximum BNS range [130].) As already discussed in Equation 15 the sensitivity increases with the beam sizes. The lower subplot of Figure 14 shows a scan of the cavity non-degeneracy, Θ_{15}, including HOM of up to order 15. One can see a general tendency for decreased cavity non-degeneracy for larger beam sizes. In addition we see stripes diagonal stripes of very low non-degeneracy, especially for small beam sizes. These stripes indicate beam sizes for which one specific HOM is exactly resonant inside the arm cavities.

The polishing accuracy of the mirror ROC sets a lower limit to the favourable mode-non-degeneracy: We require the arm cavities to be still stable, even in the case of a relative ROC deviation of 2 %, leading to the requirement: $\Theta_{15} > 0.085$. Therefore, in terms of non-degeneracy of the arm cavities it would be optimal to go for a beam size combination indicated by the colour range from orange over yellow to light green in the lower subplot of Figure 14. For smaller beam sizes the risk of accidentally hitting the resonance of one of the lower order optical modes is too high, while for larger beam sizes the cavity is too close to instability.

However, for a specific mode-non-degeneracy it is possible to maximize the sensitivity by introducing asymmetric beam sizes at the input and end mirrors as mentioned in Section 5.2.1. Along each black dashed arrows in the lower subplot of Figure 14 the cavity non-degeneracy stays constant. Drawing arrows with identical slope into the upper subplot of Figure 14, one can see that it is possible to increase the sensitivity by moving towards the upper left corner, while keeping the mode-degeneracy at a constant level.

Using the two boundaries described above, $\Theta_{15} > 0.085$, and a maximum beam size of 6.5 cm (see Section 5.2.2) we can derive the optimal beam sizes and ROC values listed in Table 5.2.4. For these set of parameters the lowest order HOM close to resonance inside the arm cavity is of order 11 [129].

5.3 Arm cavity finesse

The power enhancement inside the arm cavities is determined by their finesse, i.e. the refelctivities of the cavity mirrors and the round-trip losses inside the arm cavity. The advantage of using a high finesse for the AdV arm cavities is a reduced coupling of several noise sources, originating from within the small Michelson interferometer, to the GW channel. On the other hand, high finesse arm cavities require extremely low round-trip losses.

The current baseline value for the AdV arm cavity finesse is 885, assuming scattering losses of 37.5 ppm per mirror surface. At the moment it is not guaranteed that such low scattering losses can be achieved in a reliable and reproducible way (see Section **??**). However, the fact that the final arm cavity finesse only needs to be decided when the polished mirrors are send to be coated, gives us the chance to reevaluate the optimal arm cavity finesse for AdV, taking into account the most recent results of mirror roughness analyses from within the Virgo and also LIGO collaboration.

5.4 Signal Recycling

The term Signal Recycling [138] (SR) refers generally to a Michelson interferometer with a semi-transparent mirror in the asymmetric port. It has been developed and demonstrated over more then ten years from table-top experiments, via implementations on prototypes [137] to being used routinely in the GEO 600 detector today [136]. The main aim of Signal-Recycling is to increase the signal-to-quantum-noise ratio of the detector. Depending on the arm cavity finesse, Signal Recycling comes in two different flavours. If the arm cavities have a low finesse, Signal Recycling can be used to further *decrease* the detector bandwidth to increase the peak sensitivity. This represents to ordinal Signal Recycling configuration. Instead the arm cavities can be designed to have a very high finesse and then the Signal Recycling cavity can be tuned differently in order to *increase* the detector bandwidth again. The latter configuration is often called *resonant sideband extraction* (RSE) and represent the setup chosen for Advanced Virgo.

Figure 15 shows the effect of the Signal Recycling mirror (SRM) on the quantum-noise limited sensitivity of Advanced Virgo for various parameter options. The top plot illustrates how a low transmittance of the SRM can be used to increase the peak sensitivity by reducing the bandwidth. The lower plot shows, how the quantum-noise limited sensitivity changes shape when the SRM tuning is changed. The tuning can be easily changed during operation.

The Virgo vacuum system already includes a vacuum tank for the Signal Recycling mirror. The main challenge of Signal Recycling is the more complex control system (see Section 11). Not only does it add three new degrees of freedom (1 longitudinal and 2 alignment) but it forms a very complex split, coupled four-mirror cavity with the Power-Recycling mirror and the arm cavity input mirrors and in consequence the control signals for these mirrors can become more strongly coupled.
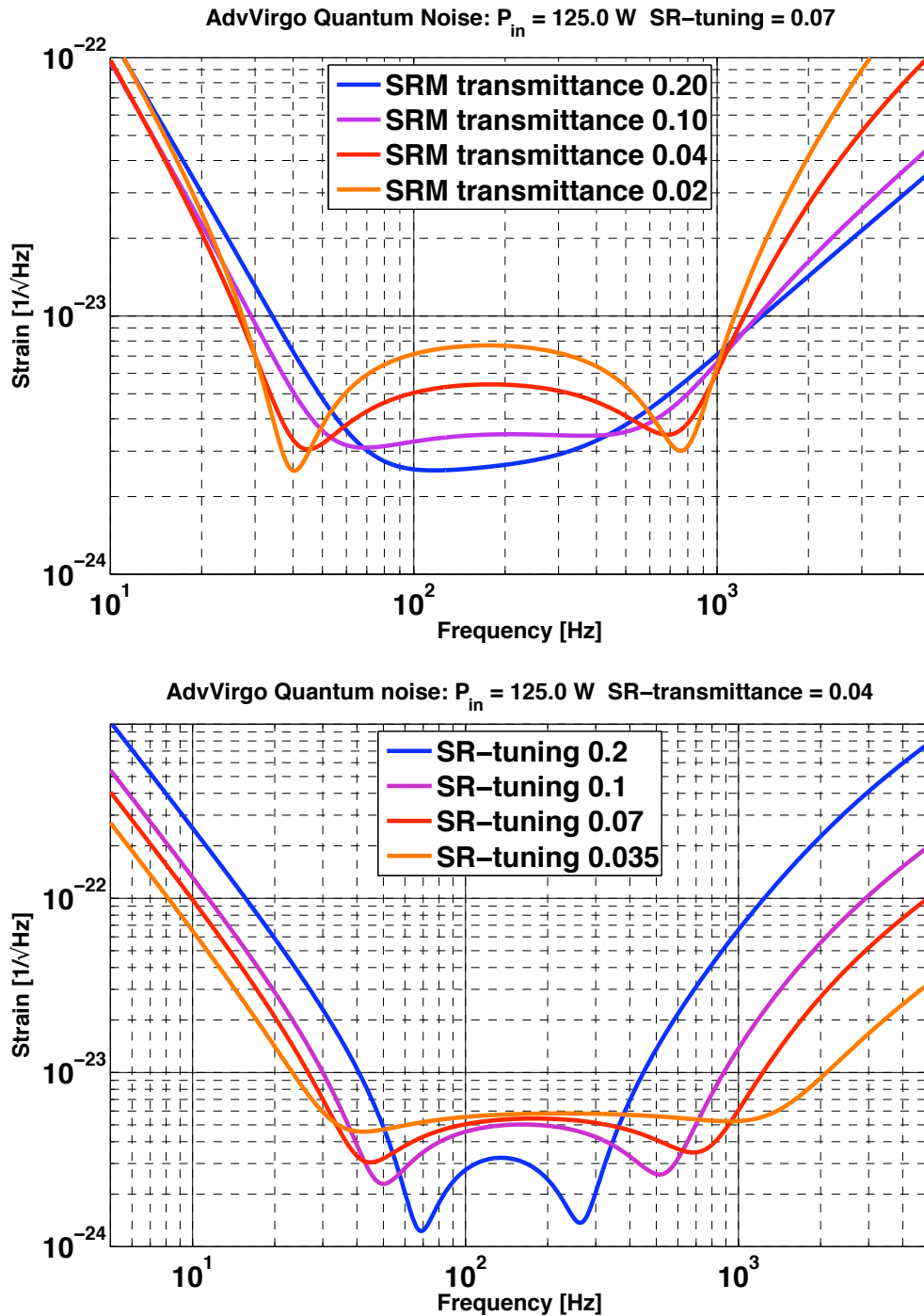
Figure 15: The two plots illustrate the impact of the two Signal-Recycling parameters, *transmittance* and *tuning* of the Signal-Recycling mirror, on the Advanced Virgo quantum noise. This shows that the exact change of the quantum noise is complex, mostly due to the optical-spring effect. However, the first order effects are that the transmittance changes the finesse of the SRC and thus the bandwidth of the detector, whereas the tuning changes the center frequency of the SRC and thus the frequency of the peak sensitivity of the detector.
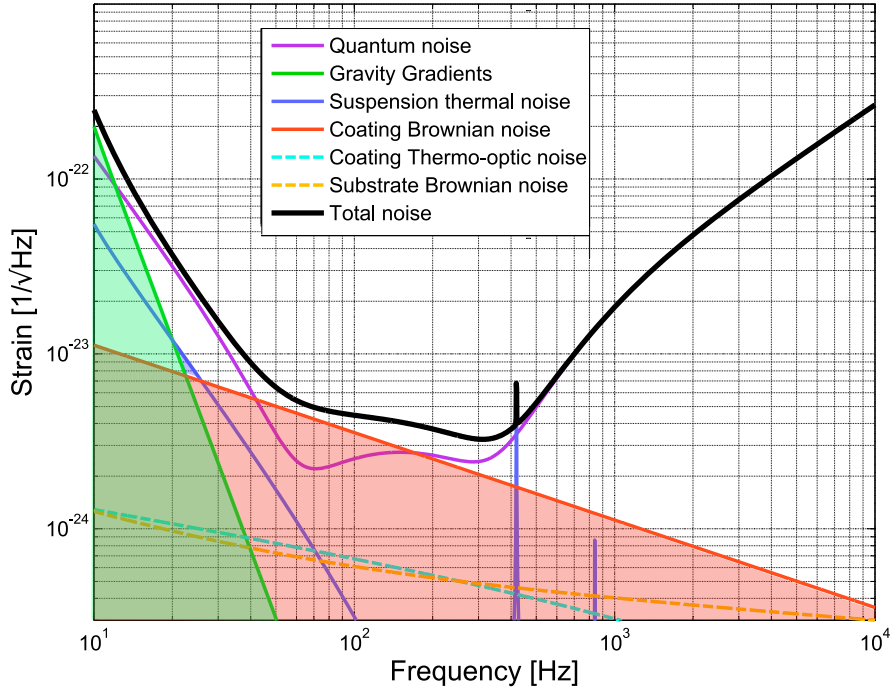
Figure 16: Fundamental noise contributions to the Advanced Virgo sensitivity. The pink trace indicates the quantum noise for one specific set of Signal Recycling parameters. It is possible to optimise the Advanced Virgo sensitivity for different figures of merit (such as BNS range), by changing the Signal Recycling detuning and the Signal Recycling mirror transmittance. The coloured areas indicate regions which are not accessible via any Signal Recycling optimisation because they are buried by other fundamental noise sources.

5.4.1 Optimisation of the Signal Recycling parameter

As shown in Figure 15, the shape as well as the level of the quantum noise varies strongly with the actual Signal Recycling parameter. Therefore, the variation of the two Signal Recycling parameter (together with the circulating optical power) offers the possibility to optimise the Advanced Virgo sensitivity for different figures of merit, such as the binary neutron star (BNS) inspiral range.

The sensitivity range available by such an optimisation is shown in Figure 16. At low frequencies the boundary is given by the level of gravity gradient noise, while in the mid and high frequency range coating Brownian noise restricts the achievable sensitivity.

Automated optimisation routines have been developed, basing on OSD-tools [128], [131] and a GWINC model of Advanced Virgo [6]. These software routines can be used for multi-parameter optimisation (Signal Recycling tuning, Signal Recycling mirror transmittance and circulating optical power) of the Advanced Virgo sensitivity for any desired figure of merit. The detector configuration optimised for binary neutron star inspiral

range [130] was chosen to be the Advanced Virgo reference configuration (see Figure 2) featuring a Signal Recycling detuning of 0.15 rad and a Signal Recycling mirror transmittance of 11 %.

5.5 Non-degenerate recycling cavities

One of the major evolutionary step during the development of the optical layout of AdV was the inclusion of non-degenerate (or stable) recycling cavities. This is also a major difference with respect to initial Virgo and initial LIGO, which have a marginally stable (or degenerate) power recycling cavity.

A Fabry-Perot cavity is stable when the transversal mode spacing is much larger than the linewidth of the cavity itself. In these kind of cavities the high-order modes cannot simultaneously build-up when the fundamental mode is resonant. On the contrary, in a degenerate cavity, the optical power is easily transferred from the fundamental mode to the higher-order modes in presence of misalignments, thermal deformation of the mirrors or any other defects in the mirror geometry.
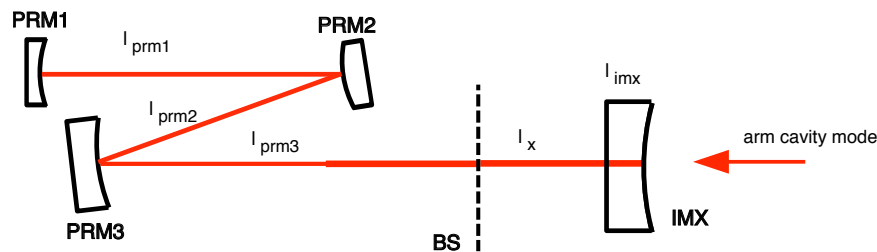

Figure 17: Simplified layout for a non-degenerate power recycling cavity, following the Advanced LIGO design. IMX represents the X-arm cavity input mirror, PRM1 is the power recycling mirror and PRM2 and PRM3 are turning mirrors that act as a kind of mode-matching telescope. PRM1 and PRM3 would be located inside the injection tower, PRM3 in the power recycling tank. The front face of IMX is shown to be flat in this picture, for the solution including a lens in the input test masses, this surface would be curved to create the lens effect.

5.6 Draft design and further steps

Todo: update this with option 2 numbers, add figure Following the Advanced LIGO design concept we have developed a set of tools to adapt this concept to AdV recycling cavities. We further have provided a draft design for the Power-Recycling cavity [135]. For the calculations an arm cavity mode with Gaussian beam parameter $q = 1400 + i275.838$ was used. The core parameters of this design are the radii of curvatures of the mirrors:

component	IMX (AR)	PRM3	PRM2	PRM1
R_c [m]	10.5	30	-1.849	2.118

The corresponding beam parameters inside the Power-Recycling cavity are:

	IMX (AR)	BS	PRM3	PRM2	PRM1
w [mm]:	50	38.5	16.5	2.17	1.77
w_0 [mm]:	0.162	0.162	0.106	0.395	0.395
z [m]:	-23.9	-18.4	-5.18	-2.49	-2.01
R_c [m]:	-23.9	-18.4	-5.18	-2.57	-2.12

The columns refer to optical surfaces inside the PRC and the rows to parameters of the beam, with w refers beam size on the respective component; w_0 and z give the beam parameters for each beam segment in the form of waist size and position; R_c is the radius of curvature of the beam's phase front. These parameters refer to the beam *leaving* the respective component. This design provides a single-trip Gouy phase of 160 degrees. The relative distances between the objects are:

	l_{prm1}	l_{prm2}	l_{prm3}	l_{x}	l_{imx}
length [m]	4.5	4.5	10.5	5.5	0.1

This results in a cavity length[6] of $L_{\mathrm{prc}} = 25.2\,\mathrm{m}$. The lengths used in this design put the optics into the existing vacuum enclosure but require a major redesign of the injection and detection bench because each of these would now need to accommodate two mirrors from the respective recycling cavity.

The draft design further includes lenses in the input test masses and thus manages to gives values for the beam sizes and curvatures very similar to the Advanced LIGO case. Further development of this design will focus on the feasibility of lenses in the input test masses, possible astigmatism in the off-axis telescopes and on finding the optimal Gouy phase for the Power- and Signal-Recycling cavities. Particular emphasis will be given to the interfaces of the core interferometer to the injection subsystem (see Section 7) and the detection subsystem (see Section 10).

---

[6] Please note that for compatibility with RF modulation frequencies the power recycling length must be adjusted to be close to 24 m. However, this has only a small influence on the cavity parameters presented here. The exact cavity length and the exact radii of curvatures will be determined at a later stage.